

FeAs₂ formation and electronic nematic ordering: an analysis in terms of structural transformations

A. Pishtshev^{1,*} and P. Rubin¹

¹*Institute of Physics, University of Tartu, Ravila 14c, 50411 Tartu, Estonia*

(Dated: April 5, 2024)

By combining DFT-based computational analysis and symmetry constraints in terms of group-subgroup relations, we analysed the formation of the native crystalline structure of loellingite FeAs₂. We showed that the ground state of the material exhibits the ordered patterns of the electronic localization which are mainly associated with iron $3d_{x^2-y^2}$ orbitals and can be characterized in terms of nematic-like ordering. The ordering is the result of the close interplay of the lattice and the electron degrees of freedom. In a structural aspect, it pursues an energy quest to select the orthorhombic crystal lattice attributed to the $Pnmm$ space group. In a charge aspect, the ordering is connected with the valence charge density redistribution that not only provides a high electronic polarizability but also gives rise to an extra-large magnitude of the negative component of the dynamical p-d charge transfer.

PACS numbers: 31.15.A-; 71.20.Ps; 63.70.+h

Keywords: pnictide, loellingite, crystal structure, electronic structure, chemical bonding

I. INTRODUCTION

The structural integrity of a bulk solid containing a transition metal (TM) element with an open $3d$ -shell is governed by a mutual balance of the driving chemical interactions. In this aspect, the direct charge transfer, the overlap of the outer orbitals, and the many-body effects of electronic correlations appear to be the most significant structure-dependent factors. On the other hand, the cooperative character of chemical bonding in the periodic lattice determines the activity of these interactions upon a wide range of length-scales. The effects of electronic correlations plays a very important role because they tend to keep an atomic format of partially filled $3d$ states. This factor causes charge localization on short-range scales and thereby gives extra opportunities for valence electrons to affect the underlying chemical structure, crystal packing geometry, and electron sharing possibilities.

Thus, the flexible theoretical characterization of the crystal design of a compound with a $3d$ TM element should greatly depend on an understanding of how the typical properties of structural geometry of the solid state may be influenced by the features of spatial localization patterns of valence electrons. In the article, using the pnictide FeAs₂ as a model example of a binary TM-nonmetal alloy we ascertain how the interplay between lattice stabilization and valence electron localization sets up interesting peculiarities of the crystal chemistry of this material. To gain full insight, we investigated the electronic properties caused by the $3d$ electrons of Fe cations in terms of possible structural transformations driven by a TM-ligand coordination. Based on the obtained results, we found that the formation of a preferred architecture of FeAs₂ is accompanied by the further utilization of Fe–Fe planar interactions with the establishment of nematic-like ordering.

II. MATERIAL, METHODS AND SIMULATION DETAILS

Loellingite belongs to a family of binary compounds (called pnictides) that contain a combination of a TM with the ligands consisting of Group 15 elements such as P, As, Sb, and Bi.¹ The orthorhombic structure of FeAs₂ is characterized by the space group $Pnmm$ (compressed marcasite phase) with lattice parameters $a=5.3012$ Å, $b=5.9858$ Å, $c=2.8822$ Å.² A study of the Fe–As phase diagram showed³ that FeAs₂ retains stability up to its melting point at 1020° C. The insulating nature of FeAs₂ was observed in resistance measurements⁴ performed for a single crystal at ambient temperatures. An estimate of the band gap made from an analysis of the experimental resistivity ρ behavior *vs.* T in terms of $\log\rho$ indicated a value of about 0.22 eV. Computational studies of the electronic structure of FeAs₂ provided information on the main features of electron bonds.⁵

To gain a deeper insight into the characteristic details of $3d$ iron (and $4p$ arsenic orbitals) and to understand the structural factors markedly affecting the electron localization in FeAs₂, we analyzed the ground state by employing DFT+U theory⁶ and the G_0W_0 approximation⁷, with an emphasis on determining the role the coordination environment plays in the genesis of the electronic subsystem. We performed spin-polarized periodic calculations using the Vienna *ab initio* simulation package (VASP)⁸ together with the potential projector augmented-wave (PAW) method.⁹ As iron belongs to the category of first-row late transition metal elements with localizable d orbitals, we determined

the Kohn-Sham (KS) eigenstates within the Perdew-Burke-Ernzerhof (PBE) GGA exchange-correlation functional¹⁰ augmented with the Hubbard U term. The approach of Dudarev *et al.*¹¹ has been used for PBE+ U calculations. The effective value of the on-site d - d Coulomb repulsion, which represents the difference of the intra-atomic (U) and exchange (J) contributions $U_{eff} = U - J$, was estimated via constrained PBE calculations based on linear response theory.¹² We found that an average U_{eff} of 1.6 eV can be applied to take into account electron correlations in the description of the FeAs₂ ground state. In accordance with experiment,² our calculations reproduced a nonmagnetic ground state. The topological features of the valence electron distributions were investigated on the base of the theoretical charge densities; a grid-based Bader analysis post-processing method,¹³ which implements the AIM ("atoms in molecules") approach¹⁴ and the electron localization function (ELF)¹⁵ have been employed. The many-body polarization effects were characterized in terms of the Born dynamical charges;¹⁶ these charges were calculated within the scheme of density functional perturbation theory.¹⁷ Analysis of the structural properties was performed by using the programs FINDSYM of the ISOTROPY Software Suite¹⁸ and VESTA.¹⁹ For visualizations of the structures and electron topologies, we applied the VESTA program. Group-subgroup sequences forming the Bärnighausen tree²⁰ were found by using the programs INDEX and SUBGROUPGRAPH²¹ hosted by the Bilbao Crystallographic Server.^{22,23}

A plane-wave basis set with a 500 eV cutoff and a Γ point centered mesh for the \mathbf{k} -point sampling have been chosen in our calculations. For cell and atom relaxations and stability analysis, \mathbf{k} -grid sampling was taken as $6 \times 6 \times 8$. G_0W_0 calculations employed a $6 \times 6 \times 10$ \mathbf{k} -point grid. The details of the electronic structure were investigated at a denser $8 \times 8 \times 12$ \mathbf{k} -point grid. The tetrahedron method with Blöchl corrections²⁴ was used for Brillouin zone integrations. Zone centered vibrational modes and elastic moduli were obtained within the frameworks of the finite differences method, as implemented in VASP.

III. RESULTS AND DISCUSSION

A. Chemical content of structural formation of FeAs₂

Although chemical considerations relate FeAs₂ to intermetallic compounds/metalloids (like NiAs₂), the material is qualified as a low-gap semiconductor. Our DFT calculations have shown that the relatively small Hubbard energy ($U_{eff} \sim 1.6$ eV) related to iron 3d electrons does not favor the metal-dielectric transition. Note also that both elements of the composition FeAs₂ possess approximately similar values of the Pauling electronegativity (1.83 for Fe and 2.18 for As). In this case, the mechanism of TM-ligand coordination, lattice structure stabilization and formation of the band gap appears an open problem when viewed from the point of view of crystal design. To reveal the key role the coordination environment plays in the genesis of the electronic structure, we considered the theoretical route of the FeAs₂ structural assembly. Starting from the chemical composition, we presumed that an assembly route of FeAs₂, written in terms of the chemical building blocks as



represents *a de novo* process under which an array of As dimers is packed into the iron framework to arrange Fe-As coordination. In a formal chemical context, the left part of this reaction corresponds to the starting mixture of the reactants, which is used in practical work, for example, in the chemical vapor transport method to grow FeAs₂ single crystals.⁴ In our approach, we modeled a couple of As atoms in terms of an intermediate dimer to be placed in the parent Fe lattice. We also assumed that the structural transformation passes the chemical content through the affinity property of rectangular lattices. This provides an optimization of atom sites via the regular scalability of the unit-cell shape/volume coupled with the recasting of arsenic positions in the coordination environment.

By using the concept of an isotropy subgroup,²⁰ we found the constraints for the structural transformations of the system. In Fig. 1, the Bärnighausen tree of possible structural relations for FeAs₂ is given, from where we decided in favor of the following set of allowed group-subgroup pairs: $Im\bar{3}m \rightarrow I4/mmm \rightarrow Immm \rightarrow Pnmm$. Based on this prediction, Fig. 2 shows the assembly route as a three-step pathway. Note that, prior to the first step, we made a tetragonal rebuilding of a single *bcc* iron lattice, $Im\bar{3}m \rightarrow I4/mmm$, via equal doubling of the cubic lattice period $a \rightarrow 2 \times 2.8274$ Å in both longitudinal directions. This manipulation preformed a superstructure of Fe atoms as a starting template qualified for the incorporation of arsenic dimers. Their initial packing arrangement proceeds by placing them into a stacked disposition, followed by a small lengthening, $2.8274 \rightarrow 2.8747$ Å, of the lattice along the tetragonal c direction. The first step ends in the formation of a putative structure featured by an orthorhombic space group $Immm$ (labeled as Phase 0). Because such a trial configuration turns out to be unstable, on the next step, As atoms are further packed to lower the ground state energy. With respect to the geometry, the subsequent repacking leads to the crossover from the I -lattice to the P -lattice and to the reduction in symmetry to the non-isomorphic subgroup $Pnmm$. Crystal stability is achieved in the coordination environment by rearrangements of the As atoms via

the As–As bonds elongation and rotation. This step forms the refined intermediate configuration (“hidden” phase labeled as Phase I) associated with the conversion of the unfavorable arsenic ‘4*h*’ sites to ‘4*g*’ ones. In the final step, the native structure of FeAs₂ (labeled as Phase II) is formed by a “square-rectangular” transformation in the planar sublattice of iron atoms. This transformation generates the difference of the in-plane lattice parameters but keeps the same *Pnmm* group.

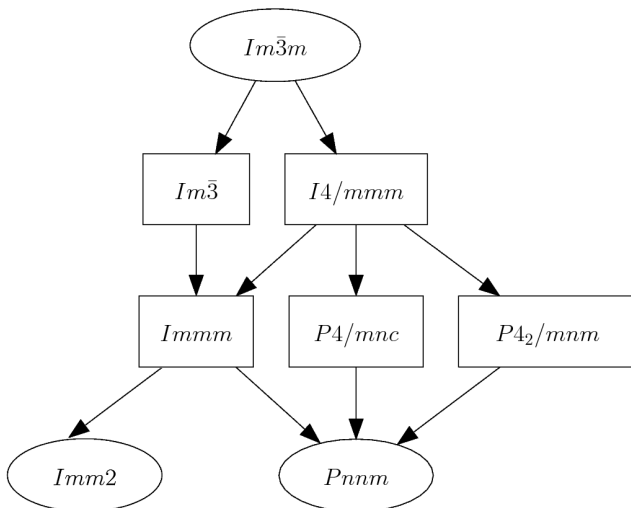


Figure 1: The Bärnighausen tree related to the loellingite structure.

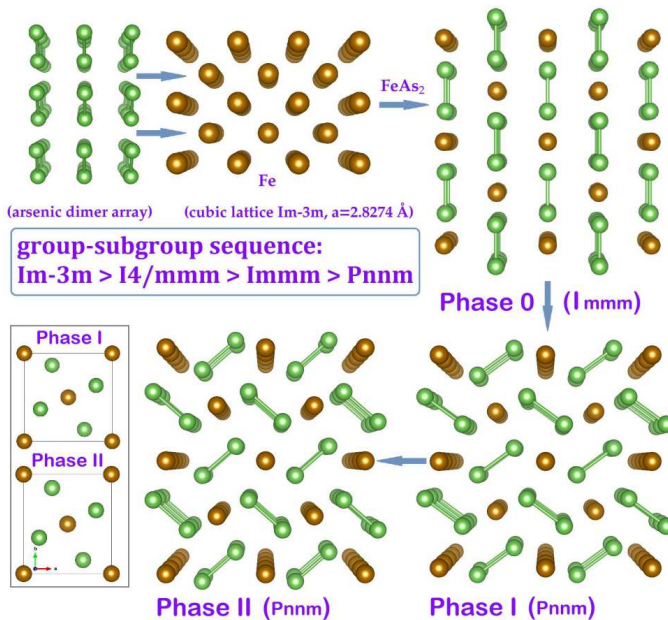


Figure 2: Flowchart of the FeAs₂ three-phase assembly between the template and the native structures. Atoms are shown as brown (Fe) and green (As). The crystallographic data are given in Appendix (Table III). The packing of Phases 0, I, and II is shown as a perspective *c*-axis plot. The common motif of all phases is a full matching of the Wyckoff positions (‘2*a*’ sites) occupied by iron atoms. The assembly utilizes the arsenic dimer array, which is disposed along the *c*-axis by fixation to the iron *z*-coordinate after dissolving in the iron framework of the *I4/mmmm* symmetry. The dimer-iron linkage occurs along one of the lattice sides as the “axial alignment” of As–As bonds. This determines the direction of the *c*-axis because of the $O_h \rightarrow D_{2h}$ reduction of the parent *Im3m* crystal symmetry and preassigns the smallest side, 2.8747 Å, of the unit cell. The differences of the total energies between Phases 0 and I, and between Phases I and II are 448 kJ/mol and 54 kJ/mol, respectively.

as shown in Fig. 1) that suggests an alternate version of As atoms packing. A performed theoretical screening predicted the possibility of a novel polymorph of FeAs_2 with lattice parameters of $a=5.425 \text{ \AA}$, $b=6.279 \text{ \AA}$, and $c=2.976 \text{ \AA}$. A Table IV of Appendix gives the set of calculated crystallographic data. The polymorph has an inverse symmetry broken orthorhombic structure characterized by the polar space group $Im2m$. To analyze stability issues, we calculated the elastic constants (the stiffness matrix is shown in Figure 3C) and the harmonic frequencies of the zone centered vibrational modes (the values are displayed in the Appendix). We found that the $Im2m$ structure fulfills the mechanical and dynamical stability tests. However, the difference in energy with respect to the native structure is strongly positive, $\Delta E_{tot} = 174 \text{ kJ/mol}$. Hence, the polymorph of the $Im2m$ symmetry cannot be thermodynamically stabilized under ambient conditions, and therefore, it is much less feasible than the experimentally observed geometry of Phase II.

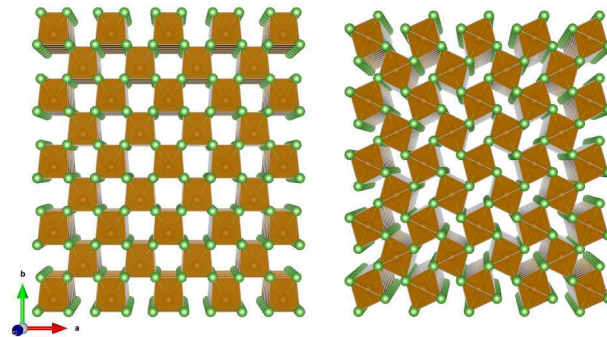


Figure 4: View of the packing scheme of the polymorph and the native phase of FeAs_2 along the c -axis. The crystal structures are depicted as a three-dimensional network composed of 1D chains of corner-sharing FeAs_6 polyhedra. FeAs_6 polyhedra are shaded in brown. The color codes are the same as in Fig. 2.

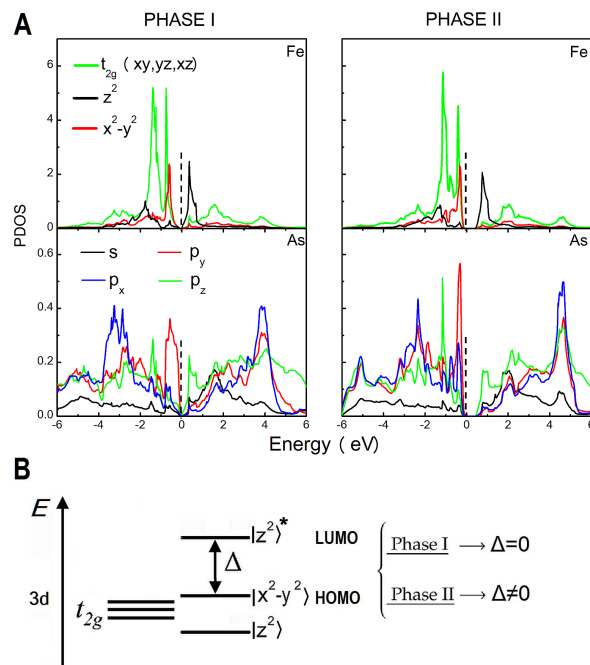


Figure 5: The differences in the electronic structures of Phases I and II obtained from the PBE+U calculations. (A) Orbital and site projected electron densities of states (PDOS). Vertical dashed lines indicate the chemical potential position. (B) An illustrative energy scheme of the e_g doublet, showing the origin of the fundamental gap (Δ) in the electron spectrum. Although actual bonding and antibonding orbitals have some hybrid character caused by the light admixture of the As p states (Fig. 5A), frontier Fe e_g orbitals make the major contribution to an orbital character of the gap.

Figure 4 illustrates the difference of the arrangement of the FeAs_6 polyhedra in the crystal structures of the polymorph and the native phase of FeAs_2 . In both geometries, one can observe the void tunnels of keystone and

rhomboidal shapes, the edges of which are formed by corner-sharing FeAs_6 polyhedra. Figure 4 also shows that just in the structure of the polymorph, the tunnels determine the largest interstice space that may present a number of preferential positions for the incorporation of dopant atoms. In the context of iron-based materials studies, this interesting fact might allow us to consider the hypothetical FeAs_2 of $Im2m$ symmetry as a possible starting compound for a theoretical design of new ternary iron pnictides.

D. Modeling of the structure-property connection

Figure 5 visualizes the respective changes in the electron subsystem of FeAs_2 in terms of the partial densities of states. Choosing *bcc* Fe as a reference point and recalling that the assembly is based on a superstructural architecture derived from the *bcc* iron lattice, one would expect, in the context of a *3d*-split configuration, a replication of the effects of atomic-like Fe-*3d* states in the electron spectrum of FeAs_2 . It appears to be nearly so, regardless of the *p-d* hybridization effects inspired by the coordination of As ligands. A comparison shows that the orbital-selective features of Fe in FeAs_2 , such as the hybridization character of a t_{2g} manifold of states and stronger localization of e_g states (Fig. 5A), demonstrate the orbital properties similar to the α -Fe electronic structure.²⁷ Furthermore, a small pseudogap in the density of the states of Phase I means that the ligand field strength is not yet sufficient to overcome hybridization effects and, hence, to completely exclude the system from the metallic range. However, as shown in Fig. 5, a change of the orbital overlap caused by the transformation Phase I \rightarrow Phase II leads to the conversion of the pseudogap into a real forbidden gap of ~ 0.4 eV. In contrast to octahedral complexes, this transformation forms a certain electronic configuration of Fe e_g states, which corresponds to an insulating state of a orbital nature (as depicted in Fig. 5B).

To confirm the presented picture of the electron states, we compared the results of our PBE+U calculations with those obtained within the G_0W_0 approximation. The G_0W_0 calculations resulted in a similar electron structure (see the PDOS dependencies shown in Fig. 10 of the Appendix), and they reproduced the value of the dielectric gap very close to that obtained by the PBE+U method.

We can further track how the bonding states of the $d_{x^2-y^2}$ symmetry underlie a particular charge ordering in the orbital sector of FeAs_2 . As schematically illustrated in the upper half of Fig. 6, the Fe atoms occupy the corners of a square with sides of length a in Phase I.

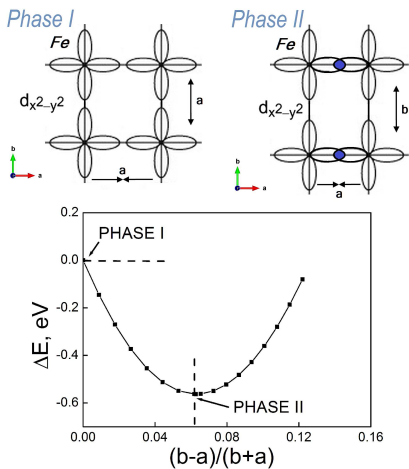


Figure 6: Characteristic patterns describing the genesis of the nematic ordering in Phase II in the orbital sector of $|x^2 - y^2 \rangle$ functions that belong to the neighboring sites of the Fe sublattice. The net of equally spaced patterns can be imagined as being formed by a projection of the $Pnmm$ lattice on the ab -plane. In the bottom half of the figure, the total energy difference with respect to Phase I vs. the (normalized) planar deformation is graphed.

The orbital overlap generated by the functions $|x^2 - y^2 \rangle$ remains identical in both planar directions. Conversely, in Phase II, where charge redistribution occurs, the full equality of the orbital overlaps between the x and y directions becomes broken because of the planar tetragonal distortion. The distortion provides the minimization of the total energy, as shown in the bottom half of Fig. 6. Based on the results of Refs.²⁸⁻³¹, this implies that in the native structure of FeAs_2 , there exists a electronic ordering of the orbital nematic origin. The nematicity scenario can be described as follows:

(i) the electron-driven Phase I \rightarrow Phase II modification implies the transition to the nematic-like state in the subsystem

of Fe $3d_{x^2-y^2}$ valence electron orbitals (so called orbital nematicity^{28,32}).

(ii) in the geometrical context, the ordering is attended with a square \rightarrow rectangular transformation, with the structural distortion featured by the difference of the planar lattice parameters ($b - a$);

(iii) in the symmetry aspect, because of some freedom provided by the coordination environment effect within the dedicated orthorhombicity, the transition from Phase I to Phase II keeps all the operations of the space group $Pnmm$ unchanged;

and (iv) in terms of the 2D internal lattice symmetry related to the ab -plane, the distortion can be formally associated with the additional reduction of the local rotational symmetry from C_4 to C_2 with respect to the uniplanar neighboring sites of the Fe sublattice. In addition, one can also emphasize that the charge aspect of the orbital nematicity is that a spatial arrangement of the Fe $3d_{x^2-y^2}$ orbitals induces charge ordering that can be characterized by the difference of the overlap integrals between neighboring Fe $d_{x^2-y^2}$ states along the x - and y - planar directions.

E. Features of the bonding architecture: an interplay of the ordering and dynamic equilibration

To further highlight the effect of coordination environment, we point out that the relevant σ - and π -interactions driving the covalent binding of ligands to the TM form an inclined disposition of As–Fe–As building blocks in the lattice. The corresponding structural motifs are shown in Fig. 7D.

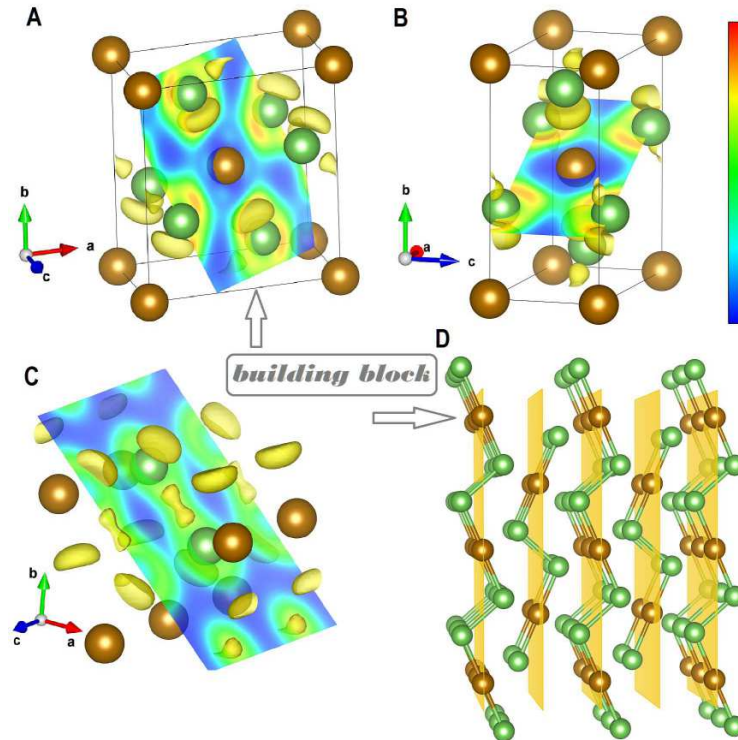


Figure 7: Valence ELF distribution patterns with isosurfaces projected onto the (A) (1.5 0.75 1.2), (B) (-1.6 3.6 0), and (C) (0.68 0.88 0) planes of the FeAs₂ crystal structure. The visualizations were evaluated at ELF= 0.661. The numerical values of the total charge partitioning, normalized between ELF= 0 and ELF= 0.8, are illustrated by the color scale between dark blue and red, respectively. The lobe-like isosurface (in yellow) displayed near the As atoms corresponds to a lone pair domain. (D) Schematic model view of the As–Fe–As building blocks in the FeAs₂ lattice; the blocks possess a linear ($D_{\infty h}$) geometry and consist of a central Fe²⁺ and two geminal As⁻. The color codes of atoms are the same as in Fig. 2.

From the aspect of dynamics the geometry of the As–Fe–As building block promotes the interplay between interatomic motions and valence electronic states. To explore how this interplay arises, note that, in the relatively low-symmetry insulators, possessing a high electronic polarizability, small variations in the spatial positions of atoms, such as vibrations, may alter the static bonding topology by involving additional displacement-induced symmetry-allowed combinations of the frontier TM d and ligand p orbitals overlapping (dynamic p - d hybridization).^{34,35} The results of our tests showed that dynamic redistribution of the valence charge density has a pronounced effect in FeAs₂. The evidence can be seen in Table II and Figures 7A-7C and 8.

Table II: Diagonal elements of the matrix of the Born effective charges (in $|e|$) along with the theoretical values of the macroscopic dielectric constant ϵ_∞ .

	x	y	z
Fe	-5.82	-5.05	-6.94
As	+2.91	+2.52	+3.49
ϵ_∞	27.0	33.0	24.4

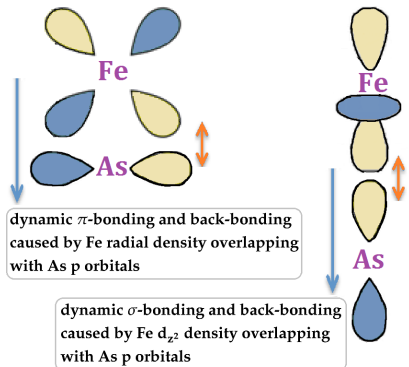


Figure 8: Schematic diagrams illustrating the dynamic dative nature of synergic bonds in terms of the π - and σ - components.

The first observation is that the Born effective charges of Table II are enormously anomalous as compared with the formal ionic charges of the ligand-field model. The second observation is based on the analysis of ELF. It displays the peculiar role that p -type lone pairs play at the vibrational contact. These s^2p^4 pairs are localized and ordered around the geminal As^- . The stereochemical activity of the pair mostly has a dynamical character, i.e., it may benefit the local delocalization through the dynamical back bonding from the ligand lone-pair to the central Fe^{2+} $3d$ states. The "virtual" transfer of the lone pair promotes a iron-reductive (arsenic oxidative) coupling that brings them an enhanced negative (positive) effective charge (Table II). Interestingly, the similar effect of "virtual" presence of a lone pair through electron-phonon coupling was considered for the Te-II phase.³⁶ Because the ligands stay coordinated to Fe at the vibrational contact, the reverse process is the donation $3d(\text{Fe}) \rightarrow 4p(\text{As})$ to restore the former localization of the lone-pair. Both processes driven by proper IR-active optical vibrations are therefore dynamically strung together by the underlying (static) bonding architecture. Thus, the strong symmetry-allowed vibrational contacts of the p and d orbitals mediate in FeAs_2 the excess negative charge-flow from the ligands onto the metal and back. This can be referred to as the dynamic component of the net charge-transfer, extra-large in magnitude but opposite in sign. Moreover, in the sense of dynamics, the back-bonding phenomenon correlates well with the fact that the Bader effective charges calculated for Fe and As have almost zero indicative values. This result simply indicates that, in the sector of the dominating covalency, "external" forcing such as the accompanying vibrations can be responsible for the additional charge asymmetry.

In the context of such an effect of dynamic equilibration, it is interesting to note that a similar situation characterized by the importance of polarization effects in the direct interaction of ligands lone pairs with the metal exists in $\text{Zn}(\text{II})$ complexes.³⁷

IV. CONCLUSION

In the present work, we performed a DFT-based analysis of the structural chemistry of the binary pnictide FeAs_2 . We showed how the electronic features caused by the behavior of the $3d$ electrons of a TM can be understood in terms of the investigation of the structural trends driven by TM-ligand interactions and the synthetic construction of a preferred architecture accompanied by using Fe-Fe bonds. Starting from a known chemical composition and having made the proper choice of symmetry constraints as an integral part of the assembling strategy, we reproduced the native architecture of the loellingite from first-principles. We also considered, for the first time, two original electronic properties of FeAs_2 , a nematic-like ordering in the subsystem of Fe $3d_{x^2-y^2}$ valence electron orbitals and an extra-large dynamic charge-transfer caused by a lone-pair configuration. The ordering results from the design-imposed structural adjustment of iron planar positions, whereas the negative dynamic charge-transfer employs the dynamical lability

of the Fe–As interactions in the covalent framework. The nematic ordering represents a macroscopic cooperative phenomenon in the electron subsystem of FeAs₂. In a sense of crystal chemistry, this is a manifestation of the structure-property relationship because the electronic topological effect is directly driven by the lattice degrees of freedom via the difference of the planar arrangements of the Fe atoms.

The interplay between the metallicity and covalence, which is a constructional feature of the FeAs₂ crystal design, may be responsible for a certain softness of the Fe–As covalent bonds. In this context, some interesting parallels with the general design principles of dynamic covalent chemistry³⁸ could be suggested. A tetragonally distorted form of *bcc* iron involved in the three-step formation pattern of FeAs₂ (Fig. 2) serves as a predesigned bulk superstructure that functions as a template to distribute ligands in the condensed phase. Preferential binding between the Fe centers and As ligands, which corresponds to the so-called "covalent capture", makes the structural motif of the template a basic part of all possible structures (including the native one) contained in the formation route. The distribution proceeds through a sequential "proof-reading" generation of two intermediate geometries because the metallic bonding of the template scales formation of covalent bonds by searching for the global minimum. The last structural correction takes place largely inside of the template and deals with the utilization of Fe–Fe bonds to provide the state with a nematic ordering. The coordination environment effect is that the corresponding coordination and stabilization processes place As atoms into favorable positions. On the other hand, the covalent capture maintains the usual labile character of Fe–As ligand interactions. Thus, the coupling of two effects, the coordination environment and dynamic equilibration, through the assembly of the most dynamically stable structure of FeAs₂ is another interesting fact in the context of the close interplay of the lattice and the electron degrees of freedom in this material.

Acknowledgments

The present work was supported by the European Regional Development Fund (Centre of Excellence "Mesosystems: Theory and Applications", TK114) and the ESF Grant No. 8991. The authors would like to thank Dr. M. Klopov for attention to this work.

V. APPENDICES

Appendix: Crystallographic data

Table III: Comparison of the relaxed equilibrium geometries (orthorhombic unit-cells, volumes, atomic positions, interatomic distances, and angles). The experimental data are given in the last column. A structure of symmetry *Immm* (Phase 0) suffers a loss of stability. At the symmetry break, which corresponds to *Immm* → *Pnmm* (Phase 0 → Phase I), the lattice constants do not change. The orthorhombic symmetry of Phases 0 and I differs by sets of As coordinates. The differences between the phases are illustrated in Fig. 9.

FeAs ₂	Phase 0 <i>Immm</i>	Phase I <i>Pnmm</i>	Phase II <i>Pnmm</i>	Expt. ² <i>Pnmm</i>
$a(\text{Å})=$	5.6548	5.6548	5.2902	5.3012(6)
$b(\text{Å})=$	5.6548	5.6548	5.9994	5.9858(5)
$c(\text{Å})=$	2.8747	2.8747	2.8747	2.8822(4)
$V(\text{Å}^3)=$	91.92	91.92	91.24	91.46
Wyckoff positions				
Fe	$2a\ 0 0 0$	$2a\ 0 0 0$	$2a\ 0 0 0$	$2a\ 0 0 0$
As	$4h\ 0 0.2967 0.5$	$4g\ 0.1838 0.3654 0$	$4g\ 0.1790 0.3616 0$	$4g\ 0.1763(10) 0.3624(7) 0$
nearest neighbor bond lengths (in Å)				
As–Fe	2.209	2.417; 2.313	2.375; 2.367	2.388(4); 2.362(4)
As–As	2.299	2.576	2.519	2.492(7)
Fe–Fe	2.875	2.875	2.875	2.882
bond angles (in grad.)				
Fe–As–Fe	81.2; 135.8	73.0; 127.9	74.5; 127.3	74.3(1); 127.0(1)
As–Fe–As	81.2; 135.8	107.0; 87.1; 92.9	105.5; 92.0; 88.0	105.7(1); 91.9(2); 88.1(2)

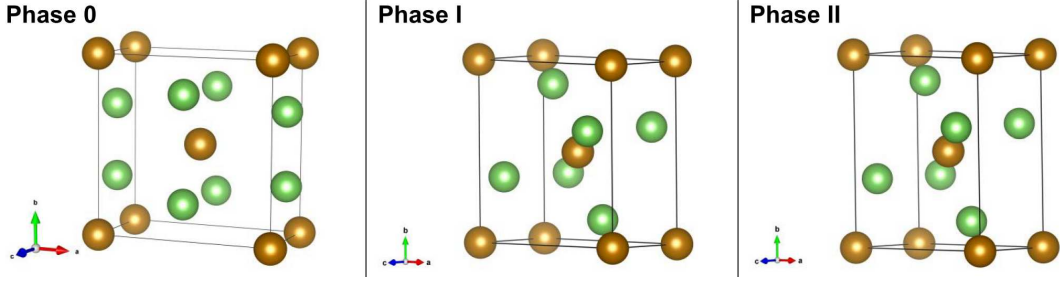


Figure 9: Schematic presentation of the unit cells. The color codes of atoms are the same as in Fig. 2.

Table IV: Relaxed equilibrium structure of a predicted polymorph of FeAs_2 featured by space group No 44. Schematic presentation of an unit cell is shown in Fig. 10.

Crystal system	Orthorhombic
Space group	$\text{Im}2\text{m}$ (44 : bca choice)
$a(\text{\AA})=$	5.425
$b(\text{\AA})=$	6.279
$c(\text{\AA})=$	2.976
Z	2
Wyckoff positions	
Fe	$2a \ 0 \ \ 0 \ \ 0$
As	$4d \ 0.2290 \ \ 0.3317 \ \ 0$

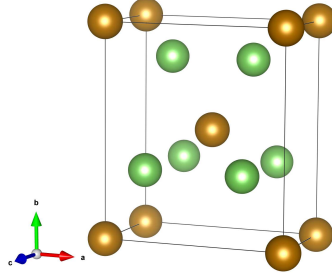


Figure 10: Schematic presentation of a unit cell of the predicted FeAs_2 polymorph with a crystallographically distinct equilibrium arrangement of As atoms. The color codes of atoms are the same as in Fig. 2.

Appendix: Dynamical stability test

List of zone centered vibrational modes calculated in the harmonic approximation (in cm^{-1}):

Phase I	109 130 130 135 189 190 204 211 227 238 254 258 280 307 325
Phase II	126 137 144 157 181 229 230 231 238 259 267 271 273 305 330
$\text{Imm}2$ polymorph	36 93 136 138 141 163 171 197 215 248 257 262 268 271 315

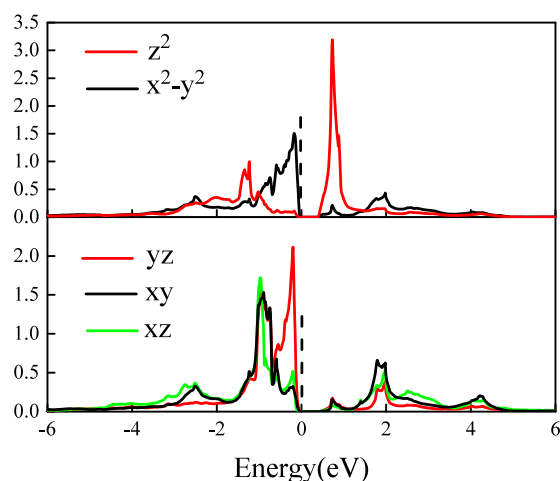
Appendix: Electron structure of the Phase II in G_0W_0 approach

Figure 11: The partial densities of d-states of Fe in the Phase II obtained by using G_0W_0 method. Vertical dashed lines indicate the chemical potential position.

* Electronic address: aleksandr.pishtshev@ut.ee

¹ N. N. Greenwood and A. Earnshaw, *Chemistry of the Elements*, (Butterworth-Heinemann, Oxford, 1997), p. 547.

² A. Kjekshus, T. Rakke and A. F. Andresen, *Acta Chem. Scand. A* **28**, 996 (1974).

³ H. Okamoto, *J. Phase Equilibria* **12**, 457 (1991).

⁴ A. K. L. Fan, G. H. Rosenthal, H. L. McKinzie and A. Wold, *J. Sol. St. Chem.* **5**, 136 1972.

⁵ K. H. Madsen, A. Bentien, S. Johnsen and B. B. Iversen, In *Proceedings of 25th International Conference on Thermoelectrics: ICT '06, Vienna, 2006*, (IEEE, New York, 2006), p. 579; J. M. Tomczak, K. Haule, T. Miyake, A. Georges and G. Kotliar, *Phys. Rev. B* **82**, 085104 (2010).

⁶ V. I. Anisimov, F. Aryasetiawan and A. I. Lichtenstein, *J. Phys.: Condens. Matter* **9**, 767 (1997).

⁷ L. Hedin, *Phys. Rev.* **139**, A796 (1965).

⁸ G. Kresse and J. Hafner, *Phys. Rev. B* **47**, 558 (1993); G. Kresse and J. Furthmüller, *Phys. Rev. B* **54**, 11169 (1996).

⁹ P. E. Blöchl, *Phys. Rev. B* **50**, 17953 (1994); G. Kresse and D. Joubert, *Phys. Rev. B* **59**, 1758 (1999).

¹⁰ J. P. Perdew, K. Burke and M. Ernzerhof, *Phys. Rev. Lett.* **77**, 3865 (1996).

¹¹ S. L. Dudarev, G. A. Botton, S. Y. Savrasov, C. J. Humphreys and A. P. Sutton, *Phys. Rev. B* **57**, 1505 (1998).

¹² M. Cococcioni, Ph.D. thesis, International School for Advanced Studies (SISSA), Trieste, 2002.

¹³ E. Sanville, S. D. Kenny, R. Smith and G. Henkelman, *J. Comp. Chem.* **28**, 899 (2007); W. Tang, E. Sanville and G. Henkelman, *J. Phys.: Condens. Matter* **21**, 084204 (2009).

¹⁴ R. Bader, *Atoms in Molecules: A Quantum Theory*, (Oxford University Press, 1994).

¹⁵ A. D. Becke and K. E. Edgecombe, *J. Chem. Phys.* **92**, 5397 (1990); A. Savin, O. Jepsen, J. Flad, O. K. Andersen, H. Preuss and H. G. von Schnering, *Angew. Chem. Int. Ed.* **31**, 187 (1992).

¹⁶ M. Born and K. Huang, *Dynamical Theory of Crystal Lattices*, (Clarendon Press, 1954).

¹⁷ M. Gajdoš, K. Hummer, G. Kresse, J. Furthmüller and F. Bechstedt, *Phys. Rev. B* **73**, 045112 (2006).

¹⁸ H. T. Stokes, D. M. Hatch and B. J. Campbell, ISOTROPY Software Suite, iso.byu.edu.

¹⁹ K. Momma and F. Izumi, *J. Appl. Cryst.* **44**, 1272 (2011).

²⁰ H. Bärnighausen, *MATCH Commun. Math. Chem.* **9**, 139 1980.

²¹ S. Ivantchev, E. Kroumova, G. Madariaga, J. M. Perez-Mato and M. I. Aroyo, *J. Appl. Cryst.* **33**, 1190 2000.

²² M. I. Aroyo, J. M. Perez-Mato, D. Orobengoa, E. Tasci, G. de la Flor and A. Kirov, *Bulg. Chem. Commun.* **43**, 183 (2011); M. I. Aroyo, J. M. Perez-Mato, C. Capillas, E. Kroumova, S. Ivantchev, G. Madariaga, A. Kirov and H. Wondratschek, *Z. Krist.* **221**, 15 (2006); M. I. Aroyo, A. Kirov, C. Capillas, J. M. Perez-Mato and H. Wondratschek, *Acta Cryst. A* **62**, 115 (2006).

²³ Bilbao Crystallographic Server, www.cryst.ehu.es.

²⁴ P. E. Blöchl, O. Jepsen and O. K. Andersen, *Phys. Rev. B* **49**, 16223 (1994).

²⁵ J. F. Nye, *Physical Properties of Crystals* (Clarendon Press, Oxford, 1985).

- ²⁶ W. Voigt, Lehrbuch der Kristallphysik, (Taubner, Leipzig, 1928).
- ²⁷ A. A. Katanin, A. I. Poteryaev, A. V. Efremov, A. O. Shorikov, S. L. Skornyakov, M. A. Korotin and V. I. Anisimov, Phys. Rev. B **81**, 045117 (2010); A. S. Belozeroov and V. I. Anisimov, J. Phys.: Condens. Matter **26**, 375601 (2014); G. Borghi, M. Fabrizio and E. Tosatti, Phys. Rev. B **90**, 125102 (2014).
- ²⁸ R. M. Fernandes, A. V. Chubukov and J. Schmalian, Nature Physics **10**, 97 (2014).
- ²⁹ R. M. Fernandes and J. Schmalian, Supercond. Sci. Technol. **25**, 084005 (2012).
- ³⁰ M. Yoshizawa, JPSJ News and Comments **12**, 3 (2015).
- ³¹ T. Iye, M.-H. Julien, H. Mayaffre, H. Horvatić, C. Berthier, K. Ishida, H. Ikeda, S. Kasahara, T. Shibauchi, and Y. Matsuda, J. Phys. Soc. Jpn. **84**, 043705 (2015).
- ³² Different aspects and scenarios of the electronic nematicity in superconducting materials based on iron pnictides and its role in the context of the interplay of structure, charge and magnetic degrees of freedom are currently the subject of intensive research work (e.g.,^{28-31,33}).
- ³³ D. Johrendt, H. Hosono, R.-D. Hoffmann, and R. Pöttgen, Z. Kristallogr. **226**, 435 (2011).
- ³⁴ S. Deng, A. Simon and J. Köhler, *Superconductivity in Complex Systems*, Structure and Bonding Vol. 114, (Springer-Verlag, Berlin, Heidelberg, 2005), p. 103.
- ³⁵ N. Kristoffel and P. Konsin, Phys. Status Solidi (B) **149**, 11 (1988); A. Bussmann-Holder, H. Bilz, and G. Benedek, Phys. Rev. B **39**, 9214 (1989); A. Pishtshev, Physica B **406**, 1586 (2011).
- ³⁶ S. Deng, J. Köhler and A. Simon, Angew. Chem. Int. Ed. **45**, 599 (2006).
- ³⁷ B. De Courcy, N. Gresh and J.-P. Piquemal, Interdiscip. Sci. Comput. Life Sci. **1**, 55 (2009); J. C. Wu, J.-P. Piquemal, R. Chaudret, P. Reinhardt and P. Ren, J. Chem. Theory Comput. **6**, 2059 (2010).
- ³⁸ S. J. Rowan, S. J. Cantrill, G. R. L. Cousins, J. K. M. Sanders and J. F. Stoddart, Angew. Chem. Int. Ed. **41**, 898 (2002).